Plastic Buckling of Axially Compressed Cylindrical Shells

S. C. BATTERMAN*
Brown University, Providence, R. I.

The plastic buckling of cylindrical shells under axial compression is studied analytically and experimentally. Attention is given to both the nonlinear and nonconservative aspects of the stress-strain relation. The effect of unloading is investigated in an exact manner for a hinge model which is proposed and in both an exact and an approximate manner for a geometrically perfect shell. Thirty tests are reported on cylindrical shells of 2024-T4 aluminum with radius to thickness ratios of 120 through 10 and length to radius ratios of 0.20 to 7. Specimens were prepared with three different types of end conditions and were tested either through a ball and socket arrangement or flat ended between smooth bearing blocks. A simple (J_2) incremental theory gives results very close to J_2 deformation theory and does predict both buckling strength and the geometry of buckling for thick and moderately thick shells.

I. Introduction

THE current literature concerned with plastic buckling problems can be summarized by saying that incremental stress-strain relations (not necessarily the simple J_2 form) are essential for a proper description of irreversible plastic behavior, that nevertheless experimentally obtained loads are in good agreement with predictions of a J_2 deformation theory, and that the role of initial imperfections and the alternate of the classical stability approach are unclear. It is not surprising that controversy exists over plastic buckling problems when complete understanding of some fundamental elastic buckling problems, which are far easier to handle analytically, still is lacking.

Prior to Shanley's famous paper[1] in 1947, many developments had already taken place in the plastic buckling of plate and shell structures. References to and summaries of the earlier developments can be found in Timoshenko and Gere.[2] In 1938, 1947, and 1949, Bijlaard[3–5] presented analytical generalizations of Engesser's tangent modulus theory for the plastic buckling of plates and shells. For the compressed cylindrical shell, Bijlaard concluded that the diamond shaped or circumferential wave mode of buckling required a higher load than the axisymmetric mode, and that loads predicted by a deformation theory of plasticity agreed very well with experiments. As part of a broader study, Gerard[6] reconsidered the buckling problem and reached essentially the same conclusions as Bijlaard. Both Gerard and Bijlaard postulated the existence of initial imperfections to allow the material to be loading at all times and so permit the use of a deformation theory as a good approximation.

Recently, Lee[7] attempted to bring predictions of an incremental theory into closer agreement with tests by considering the effects of initial imperfections on the loading process and in the nonlinear strain-displacement relations. His results appeared to show that an incremental theory, which is required on both mathematical and physical grounds, drastically overestimated the buckling strength, whereas the J_2 deformation theory predicted it quite well. Unfortunately, Lee assumed a circumferential wave mode of initial imperfection and subsequent deflection, although all of his test specimens, except one, buckled into an axisymmetric mode.

A 1950 paper which apparently has been overlooked by previous investigators is that of Kuranishi.[8] This paper represents a substantial contribution since unloading was accounted for in an approximate manner and an incremental theory was shown to correlate well with experiments.

There is no doubt as to the necessity of an incremental theory of plasticity because of the irreversibility of plastic action. However, this does not rule out the use of deformation theory which is essentially a nonlinear elastic theory. In situations when there is no unloading and the loading path is nearly radial, deformation theory should offer a good approximation to the corresponding incremental theory result.[9] Particularly in buckling problems, deformation theories are made to appear somewhat more rigorous by differentiating total stress-strain laws and thus emerging with rate forms that bear some resemblance to incremental theory relations. Budiansky[10] has shown that, for a simple J_2 theory, plastic strain rates obtained by differentiating a total stress-strain law do not satisfy Drucker's stability requirement[11] that forms a basis for the physical soundness of a plasticity theory. In fact, in order to satisfy Drucker's requirements, the loading condition $J_2 > 0$ must be abandoned and instead a corner introduced in the loading surface. Even with a corner appearing, the loading path must be restricted to lie within the hypercone generated by the tangents to the loading surface at the corner. These real restrictions and other evidence against deformation theories[12–14] often are overlooked in analyses that claim to establish the physical and mathematical validity of deformation theories in buckling problems.

Although all available evidence points to the necessity of an incremental theory, predictions of buckling stresses using an incremental theory often bear little resemblance to experimentally obtained loads, whereas deformation theory predictions are excellent in general. Onat and Drucker[15] examined this paradox. They showed that for the compressed cruciform section, or the equivalent plate problem, which fails by twisting, very small and therefore unavoidable imperfections in shape do account for the paradox. Small imperfections are needed in the cruciform problem in order to activate other than a purely elastic response to shear, Fig. 1.

Observed plastic buckling loads are maximum loads corresponding to some imperfection in geometry or dynamic disturbance.[16] The classical condition of neutral equilibrium of the idealized perfect system under constant load defines another critical load. The relevance of this critical load to

Received May 20, 1964; revision received May 20, 1964. The author is very grateful to D. C. Drucker for his aid and advice throughout the entire investigation; to Brown University for the Corinna Borden Keen Research Fellowship, which permitted uninterrupted work and concentration during the period when the major portion of this investigation was completed; and to the National Science Foundation and the Advanced Research Projects Agency for support under Grants GP-1115 and SD-86, respectively, to Brown University.

* Instructor of Engineering; now Assistant Professor of Applied Mechanics, University of Pennsylvania, Philadelphia, Pa. Member AIAA.

the observed buckling load is not always obvious.[9, 16] Shanley demonstrated conclusively that disturbances all along the loading path must be considered and the basic question is how the deflections grow with increasing load. However, actual calculations employing the Shanley concept and accounting for both the nonlinear and nonconservative aspects of the stress-strain relation are difficult and tedious even for the simplest of cases, e.g., columns. One merit of calculations based on the more popular classical stability concept is that this critical load is far easier to obtain than the maximum load that the system can withstand. Unloading must, of course, still be accounted for so that the load obtained from classical concepts is in itself difficult to calculate.

In cases of plastic buckling, as well as elastic, classical stability concepts probably are of predictive value for real materials where a curve of load vs some characteristic deformation exhibits a flat plateau-like region and then either rises gently or falls off in a gradual manner after a maximum load is attained. Typical load-deformation curves obtained from tests that will be described in detail later are shown in Fig. 2. On the basis of these curves alone, all that can be said is that, for radius to thickness (R/h) values up to more than 20 but less than 45, classical concepts should prove meaningful. Clearly, for R/h values in the vicinity of 85, any analysis based on bifurcation occurring under constant load will lead to erroneous results. Initial imperfections would be expected to have a large effect in this range.

If the difference in predictions between classical buckling occurring with unloading taking place from that with no unloading is large, then the effect of geometric imperfections of shape or other unavoidable disturbances will be significant and perhaps enormous.[15, 16] If this difference between loads is small, it does not necessarily follow that the effect of imperfections will be small. However, for the axially compressed cylindrical shell the main role of initial imperfections in an analysis is to provide a mechanism that allows loading to occur at all times in most of the shell.[7, 17, 18] The actual spread between buckling loads calculated for the perfect system with unloading occurring from that with no unloading will indeed be shown to be small. Hence, it is reasonable to expect that the effect of geometric imperfections on the buckling load will be small. In addition, when a perfect shell buckles under pure compression, plastic moduli are activated in both the axial and circumferential directions, Fig. 1.

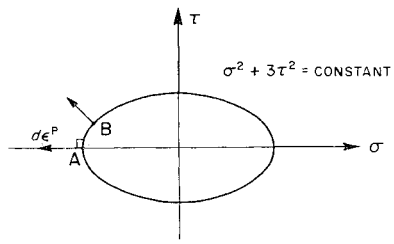

a) PERFECT CRUCIFORM - IF BUCKLING OCCURRED AT POINT A THE RESPONSE TO SHEAR WOULD BE PURELY ELASTIC. INITIAL IMPERFECTION MOVES THE STRESS POINT TO A NEIGHBORING POSITION B WITH ITS ACCOMPANYING PLASTIC RESPONSE TO SHEAR

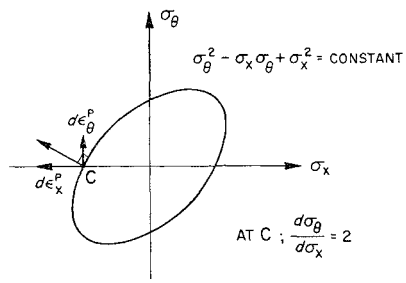

b) PERFECT CYLINDER - BUCKLING OCCURRING AT POINT C. PLASTIC INCREMENTS OF STRAIN $d\epsilon_x^p$ AND $d\epsilon_\theta^p$

Fig. 1 Mises ellipses.

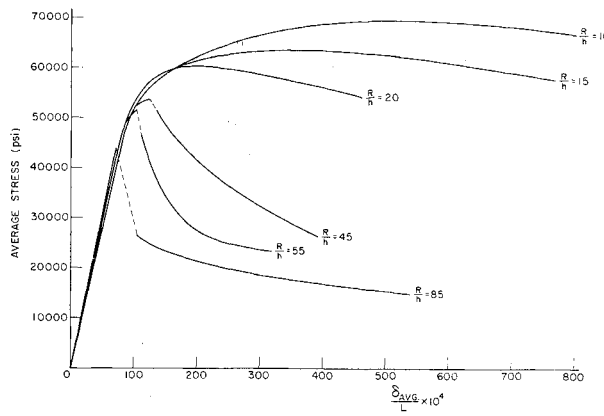

Fig. 2 Average stress vs average head movement.

II. Analysis

A. General Remarks

A previous study indicated that rate equations of equilibrium provide a natural and rational means of investigating buckling problems.[19] Specializing the general rate equations of equilibrium for axisymmetric shells to a geometrically perfect cylindrical shell, of radius R and thickness h buckling under a pure axial compression, we obtain

$$R\frac{d^2\dot{M}_x}{dx^2} + RN\frac{d^2v_n}{dx^2} - \dot{N}_\theta = 0 \qquad (1)$$

where $\dot{M}_x$ and $\dot{N}_\theta$ are, respectively, the rates of change of the meridional bending moment and circumferential membrane force measured per unit length of middle surface (Fig. 3), v_n is the incipient buckling velocity normal to the middle surface

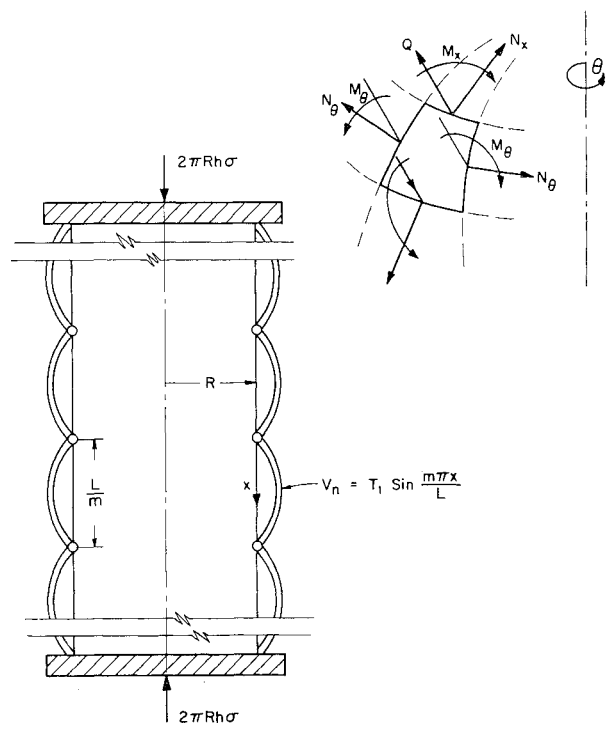

Fig. 3 Sign convention and hinge model.

measured positive inward toward the axis of the shell, x is the length coordinate measured along a generator of the cylinder, and $N = \sigma h$ where σ is the compressive stress at which buckling occurs.

The generalized rates of strain of the middle surface are

$$\begin{aligned} \dot{e}_\theta &= -v_n/R \qquad \dot{e}_x = dv_x/dx \\ \dot{\kappa}_x &= d^2v_n/dx^2 \qquad \dot{\kappa}_\theta = 0 \end{aligned} \tag{2}$$

where v_x is the incipient buckling tangential velocity measured along a generator. We remark that $\dot{e}_x$ and $\dot{e}_\theta$ are the rates of change of extensions in the axial (meridional) and circumferential directions, respectively, whereas $\dot{\kappa}_x$ is exactly equal to the rate of change of curvature in the meridional plane, and the rate of change of curvature of the middle surface in the circumferential direction is $-(\dot{e}_\theta/R)$ (see Ref. 19).

To determine expressions for the buckling stress, discussion will be restricted to the isotropic hardening J_2 incremental theory (associated with the names of Maxwell, Huber, and von Mises) and to the isotropic hardening J_2 deformation theory of plasticity. Results obtained are representative of those that would be obtained by using any reasonable theory, although in fact plastic deformation of metals occurs anisotropically. The principal objective of obtaining reasonable engineering predictions to the buckling stress does not require a detailed discussion of plastic stress-strain relationships, although such considerations are extremely important in their own right.

According to the J_2 incremental theory, the plastic strain rate is given by

$$\begin{aligned} \dot{\epsilon}_{ij}^{\,p} &= F(J_2)s_{ij}\dot{J}_2 \qquad \dot{J}_2 > 0 \\ \dot{\epsilon}_{ij}^{\,p} &= 0 \qquad \dot{J}_2 \leq 0 \end{aligned} \tag{3}$$

where

$$\begin{aligned} s_{ij} &= \sigma_{ij} - \tfrac{1}{3}\sigma_{kk}\delta_{ij} \\ J_2 &= \tfrac{1}{2}s_{ij}s_{ij} \end{aligned}$$

and σ_{ij} is the stress tensor, δ_{ij} is the Kronecker delta and repeated indices denote summation over the range of values of the index.

Combining (3) with an isotropic linear elastic response in regions of loading, $\dot{J}_2 > 0$, we have

$$\dot{\epsilon}_{ij} = (1/E)[(1+\nu)\dot{\sigma}_{ij} - \nu\dot{\sigma}_{kk}\delta_{ij}] + F(J_2)s_{ij}\dot{J}_2 \tag{4}$$

where E and ν are, respectively, Young's modulus and Poisson's ratio, and $F(J_2)$ can be determined from a simple tension test:

$$F(J_2) = (3/4J_2)[(1/E_T) - (1/E)]$$

E_T is the ordinary tangent modulus obtained from the uniaxial stress strain curve.

According to J_2 deformation theory, the plastic strain rate obtained by differentiation of a total stress-strain law is[10]

$$\dot{\epsilon}_{ij}^{\,p} = \frac{3}{2}\left(\frac{1}{E_S} - \frac{1}{E}\right)\dot{s}_{ij} + \frac{3}{4}s_{ij}\left(\frac{1}{E_T} - \frac{1}{E_S}\right)\frac{\dot{J}_2}{J_2} \tag{5}$$

where E_S is the ordinary secant modulus.

Combining (5) with a linear elastic response gives

$$\dot{\epsilon}_{ij} = \frac{1}{E}[(1+\nu)\dot{\sigma}_{ij} - \nu\dot{\sigma}_{kk}\delta_{ij}] + \frac{3}{2}\left(\frac{1}{E_S} - \frac{1}{E}\right)\dot{s}_{ij} + \frac{3}{4}s_{ij}\left(\frac{1}{E_T} - \frac{1}{E_S}\right)\frac{\dot{J}_2}{J_2} \tag{6}$$

An observation of Bijlaard which will prove useful is to note that if in (6) one sets $E_S = E$, then (6) reduces to (4).

The strain rates at a distance ξ, measured positive inward from the middle surface, are given by

$$\dot{\epsilon}_x = \dot{e}_x - \xi\dot{\kappa}_x \qquad \dot{\epsilon}_\theta = \dot{e}_\theta \tag{7}$$

which are consistent with the assumptions normally made in thin-shell theory.

Stress rate resultants are related, in the usual manner, to the stress rates by

$$\begin{aligned} \dot{N}_\theta &= \int_{-h/2}^{h/2}\dot{\sigma}_\theta d\xi \qquad \dot{M}_\theta = -\int_{-h/2}^{h/2}\dot{\sigma}_\theta\xi d\xi \\ \dot{N}_x &= \int_{-h/2}^{h/2}\dot{\sigma}_x d\xi \qquad \dot{M}_x = -\int_{-h/2}^{h/2}\dot{\sigma}_x\xi d\xi \end{aligned} \tag{8}$$

B. No Unloading

When buckling commences from a state of uniaxial compression ($\sigma_x = -\sigma$), the stress rates in regions of loading are

$$\begin{aligned} \dot{\sigma}_x &= \frac{E}{(5-4\nu)\lambda - (1-2\nu)^2}[(\lambda+3)\dot{\epsilon}_x + 2(\lambda - 1 + 2\nu)\dot{\epsilon}_\theta] \\ \dot{\sigma}_\theta &= \frac{E}{(5-4\nu)\lambda - (1-2\nu)^2}[4\lambda\dot{\epsilon}_\theta + 2(\lambda - 1 + 2\nu)\dot{\epsilon}_x] \end{aligned} \tag{9}$$

for incremental theory, where $\lambda = E/E_T$, and

$$\begin{aligned} \dot{\sigma}_x &= \frac{E}{(3\psi + 2 - 4\nu)\lambda - (1-2\nu)^2} \times \\ &\qquad [(\lambda + 3\psi)\dot{\epsilon}_x + 2(\lambda - 1 + 2\nu)\dot{\epsilon}_\theta] \\ \dot{\sigma}_\theta &= \frac{E}{(3\psi + 2 - 4\nu)\lambda - (1-2\nu)^2} \times \\ &\qquad [4\lambda\dot{\epsilon}_\theta + 2(\lambda - 1 + 2\nu)\dot{\epsilon}_x] \end{aligned} \tag{10}$$

for deformation theory where $\psi = E/E_S$.

In analogy with one aspect of tangent modulus theory for columns assume that the entire thickness of the shell is loading at buckling, i.e., $\dot{J}_2 > 0$ everywhere. For J_2 incremental theory, we find

$$\left.\begin{aligned} \dot{N}_\theta &= D_I\left[\lambda\dot{e}_\theta + \frac{(2\nu + \lambda - 1)}{2}\dot{e}_x\right] \\ \dot{N}_x &= D_I\left[\frac{\lambda+3}{4}\dot{e}_x + \frac{(2\nu+\lambda-1)}{2}\dot{e}_\theta\right] \\ \dot{M}_\theta &= K_I[(2\nu + \lambda - 1)/2]\dot{\kappa}_x \\ \dot{M}_x &= K_I[(\lambda+3)/4]\dot{\kappa}_x \end{aligned}\right\} \tag{11}$$

where

$$\begin{aligned} D_I &= \frac{4Eh}{(5-4\nu)\lambda - (1-2\nu)^2} \\ K_I &= \frac{Eh^3}{3[(5-4\nu)\lambda - (1-2\nu)^2]} \end{aligned}$$

and for J_2 deformation theory,

$$\left.\begin{aligned} \dot{N}_\theta &= D_d\left[\lambda\dot{e}_\theta + \frac{(2\nu + \lambda - 1)}{2}\dot{e}_x\right] \\ \dot{N}_x &= D_d\left[\frac{\lambda + 3\psi}{4}\dot{e}_x + \frac{(2\nu+\lambda-1)}{2}\dot{e}_\theta\right] \\ \dot{M}_\theta &= K_d\frac{(2\nu + \lambda - 1)}{2}\dot{\kappa}_x \\ \dot{M}_x &= K_d\frac{(\lambda + 3\psi)}{4}\dot{\kappa}_x \end{aligned}\right\} \tag{12}$$

where

$$\begin{aligned} D_d &= \frac{4Eh}{(3\psi + 2 - 4\nu)\lambda - (1-2\nu)^2} \\ K_d &= \frac{Eh^3}{3[(3\psi + 2 - 4\nu)\lambda - (1-2\nu)^2]} \end{aligned}$$

Setting $\psi = 1$ ($E_S = E$) reduces (12) to (11), and setting $\lambda = \psi = 1 (E_T = E_S = E)$ reduces (11) and (12) to the expressions commonly used in the theory of thin elastic axisymmetric cylindrical shells.[20]

Combining (1, 2, and 11), and imposing the classical condition of neutral equilibrium at constant load, $\dot{N}_x = 0$, leads to the differential equation governing the incipient velocity field for the J_2 incremental theory case:

$$K_I \frac{(\lambda + 3)}{4} \frac{d^4 v_n}{dx^4} + N \frac{d^2 v_n}{dx^2} + \frac{4Eh}{(\lambda + 3)R^2} v_n = 0 \quad (13)$$

The nontrivial solution to (13) for the boundary conditions corresponding to a simply supported cylinder of length L

$$x = 0, x = L: \quad v_n = 0, \dot{M}_x = 0$$

is

$$v_n = T_1 \sin(m\pi x/L) \quad (14)$$

where T_1 is an arbitrary constant and m is an integer defined by

$$\frac{m\pi}{L} = \frac{2}{[hR(\lambda + 3)]^{1/2}} \{3[(5 - 4\nu)\lambda - (1 - 2\nu)^2]\}^{1/4} \quad (15)$$

Furthermore, the critical load under which (14) and (15) occurs is given by

$$N_{\tan} = \sigma_{\tan} h = \frac{2Eh^2}{R} \frac{1}{\{3[(5 - 4\nu)\lambda - (1 - 2\nu)^2]\}^{1/2}} \quad (16)$$

Since Eqs. (13–16) were derived on the tacit assumption that at buckling $\dot{J}_2 = (\sigma/3)(\dot{\sigma}_\theta - 2\dot{\sigma}_x) > 0$, it remains to check how closely this assumption is met. In terms of the solutions (14) and (15) the loading condition implies

$$-v_n \left[\frac{(5 - 4\nu)\lambda - (1 - 2\nu)^2}{(\lambda + 3)R} + \xi(2 - \nu) \left(\frac{m\pi}{L} \right)^2 \right] > 0 \quad (17)$$

For an outward wave $v_n < 0$ we find that loading does indeed occur over the entire thickness if buckling occurs at $\lambda > \lambda_{cr}$ where

$$\lambda_{cr} = [12(2 - \nu)^2 + (1 - 2\nu)^2]/(5 - 4\nu) \quad (18)$$

or for

$$\nu = 0.5 \qquad \lambda_{cr} = 9$$
$$\nu = 0.33 \qquad \lambda_{cr} = 9.13$$
$$\nu = 0 \qquad \lambda_{cr} = 9.8$$

For an inward wave $v_n > 0$, the inequality (17) cannot be satisfied at $\xi \geq 0$. If $\xi = -h/2$, (17) is satisfied if $\lambda < \lambda_{cr}$. Thus for the perfect cylinder, buckling under constant load, the assumption of loading is an excellent one for the outward waves but is very poor for the inward waves.

It is clear that, although the solution to the buckling problem has not been found, Eqs. (14–16) can be interpreted as the solution corresponding to the following model: for a cylinder of given dimensions, place momentless hinge circles at the zeros of the velocity field (14). If buckling commences at a value of $\lambda > \lambda_{cr}$, the cylinder will then buckle under the critical load (16) into a series of outward half sine waves, Fig. 3. Emphasis must be directed to the fact that for a cylinder of given dimensions only a very special spacing of hinge circles is considered, i.e., a distance (L/m) apart. Although this appears restrictive, it rigorously leads to the result that an actual perfect cylinder cannot be weaker than the hinge model.

Reconsidering the buckling problem under constant load, with no unloading, using the J_2 deformation theory relations (12) leads to the following:

$$v_n = T_2 \sin(m_d \pi x/L) \quad (19)$$

$$\frac{m_d \pi}{L} = \frac{2}{[hR(\lambda + 3\psi)]^{1/2}} \times \{3[(3\psi + 2 - 4\nu)\lambda - (1 - 2\nu)^2]\}^{1/4} \quad (20)$$

$$N_d = \sigma_d h = \frac{2Eh^2}{R} \frac{1}{\{[(3\psi + 2 - 4\nu)\lambda - (1 - 2\nu)^2]\}^{1/2}} \quad (21)$$

For the case of $\nu = \frac{1}{2}$, (20) and (21) are identical to the analogous expressions derived by Gerard.[6]

Although the loading condition $\dot{J}_2 > 0$ is no longer meaningful for the deformation theory,[10] for completeness, it can be shown that in the outward waves $\dot{J}_2 > 0$ is satisfied if $\lambda > \lambda_{cr}{}^d$ where

$$\lambda_{cr}{}^d = \frac{3(1 + 3\psi - 2\nu)^2 + (1 - 2\nu)^2}{3\psi + 2 - 4\nu} \quad (22)$$

If (22) is accepted at face value, then it is still more restrictive than the incremental theory expression (18). Consider the Ramberg-Osgood stress-strain relationship

$$\epsilon = (\sigma/E) + (\sigma/E_0)^n \quad (23)$$

where E, E_0 and n are material constants. Satisfying (22) requires $n > 9$, that is, (22) is equivalent to placing restrictions on the flatness of the uniaxial stress-strain curve. Expression (18) requires only the very nominal restriction that the tangent modulus fall off to about $\frac{1}{9}$ of Young's modulus.

C. Unloading

The need for assessing the effect of unloading on the buckling load is now evident. Attention in this section will be devoted solely to incremental theory and is analogous to reduced modulus theory for columns and plates.[21, 12]

It is not difficult to show that the surface $\xi = \xi_0$ separates the regions of loading and unloading in the shell where

$$\xi_0 = \frac{(2 - \nu)\dot{e}_x + (2\nu - 1)\dot{e}_\theta}{(2 - \nu)\dot{\kappa}_x} \quad (24)$$

and regions of loading are defined by

$$\xi > \xi_0 \qquad \text{for} \qquad \dot{\kappa}_x > 0$$
$$\xi < \xi_0 \qquad \text{for} \qquad \dot{\kappa}_x < 0 \quad (25)$$

Separate evaluation of the stress rate resultants must be carried out for $\dot{\kappa}_x > 0$ and $\dot{\kappa}_x < 0$. Consider $\dot{\kappa}_x > 0$ first. According to (25), $\xi > \xi_0$ is the region of loading and $\xi < \xi_0$ must therefore be the region of unloading. Using (9) in the region of loading and a purely elastic response in the region of unloading gives

$$\left.\begin{aligned}
\dot{N}_x &= \frac{E}{1 - \nu^2} \left[h(\dot{e}_x + \nu \dot{e}_\theta) + c \frac{(2 - \nu)^2}{2} \dot{\kappa}_x \left(\frac{h}{2} - \xi_0 \right)^2 \right] \\
\dot{N}_\theta &= \frac{E}{1 - \nu^2} \left[h(\dot{e}_\theta + \nu \dot{e}_x) + c \frac{(2 - \nu)(2\nu - 1)}{2} \dot{\kappa}_x \left(\frac{h}{2} - \xi_0 \right)^2 \right] \\
\dot{M}_x &= \frac{E\dot{\kappa}_x}{1 - \nu^2} \left\{ \frac{h^3}{12} - c(2 - \nu)^2 \left[\frac{h^3}{24} - \xi_0 \frac{h^2}{8} + \frac{\xi_0^3}{6} \right] \right\} \\
\dot{M}_\theta &= \frac{E\dot{\kappa}_x}{1 - \nu^2} \left\{ \frac{\nu h^3}{12} - c(2 - \nu)(2\nu - 1) \times \left[\frac{h^3}{24} - \xi_0 \frac{h^2}{8} + \frac{\xi_0^3}{6} \right] \right\}
\end{aligned}\right\} \quad (26)$$

where

$$c = \frac{\lambda - 1}{(5 - 4\nu)\lambda - (1 - 2\nu)^2}$$

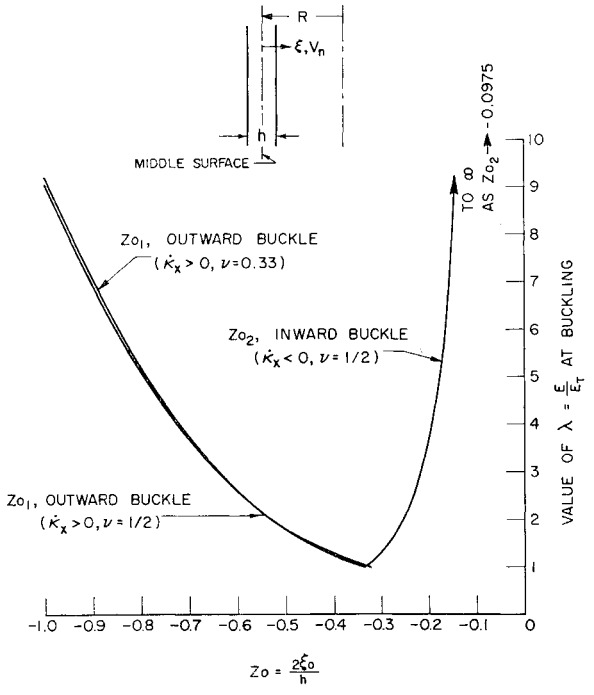

Fig. 4 Zo vs $\lambda = E/E_T$ at buckling.

In a similar manner, for $\dot{\kappa}_x < 0$,

$$\left.\begin{aligned}
\dot{N}_x &= \frac{E}{1-\nu^2}\left[h(\dot{e}_x + \nu\dot{e}_\theta) - c\,\frac{(2-\nu)^2}{2}\,\dot{\kappa}_x\left(\frac{h}{2}+\xi_0\right)^2\right] \\
\dot{N}_\theta &= \frac{E}{1-\nu^2}\left[h(\dot{e}_\theta + \nu\dot{e}_x) - c\,\frac{(2-\nu)(2\nu-1)}{2}\,\dot{\kappa}_x\left(\frac{h}{2}+\xi_0\right)^2\right] \\
\dot{M}_x &= \frac{E\dot{\kappa}_x}{1-\nu^2}\left\{\frac{h^3}{12} - c(2-\nu)^2\left[\frac{h^3}{24} + \xi_0\frac{h^2}{8} - \frac{\xi_0^3}{6}\right]\right\} \\
\dot{M}_\theta &= \frac{E\dot{\kappa}_x}{1-\nu^2}\left\{\frac{\nu h^3}{12} - c(2-\nu)(2\nu-1)\times 2-\nu\left[\frac{h^3}{24} + \xi_0\frac{h^2}{8} - \frac{\xi_0^3}{6}\right]\right\}
\end{aligned}\right\} \quad (27)$$

Combining (1, 26, 27, and 24) coupled with the classical condition $\dot{N}_x = 0$ leads to the following equations: for $\dot{\kappa}_x > 0$,

$$\frac{Eh^3}{12(1-\nu^2)}\left\{\left[1 - \frac{c(2-\nu)^2}{4}(2 - 3z_0 + z_0^3)\right]\frac{d^4v_n}{dx^4} - \frac{3c(2-\nu)^2}{2}\frac{d^3v_n}{dx^3}(z_0^2-1)\frac{dz_0}{dx} + \frac{3c(2-\nu)^2}{4}\frac{d^2v_n}{dx^2}\left[-2z_0\left(\frac{dz_0}{dx}\right)^2 + (1-z_0^2)\frac{d^2z_0}{dx^2}\right]\right\} + N\frac{d^2v_n}{dx^2} + \frac{Eh}{R}\left[\frac{v_n}{R} + \frac{ch(2-\nu)}{8}(1-z_0)^2\frac{d^2v_n}{dx^2}\right] = 0 \quad (28)$$

$$\frac{d^2v_n}{dx^2} + \frac{f_1(z_0, c)}{Rh}v_n = 0 \quad (29)$$

where

$$f_1(z_0, c) = -\frac{2(1-\nu^2)}{(2-\nu)\left[\frac{c(2-\nu)^2}{4}(1-z_0)^2 + z_0\right]} \quad (30)$$

and z_0 is the nondimensional coordinate

$$z_0 = \xi_0/(h/2) \qquad |z_0| \le 1 \quad (31)$$

For $\dot{\kappa}_x < 0$,

$$\frac{Eh^3}{12(1-\nu^2)}\left\{\left[1 - \frac{c(2-\nu)^2}{4}(2 + 3z_0 - z_0^3)\right]\frac{d^4v_n}{dx^4} + \frac{3c(2-\nu)^2}{2}\frac{d^3v_n}{dx^3}(z_0^2-1)\frac{dz_0}{dx} + \frac{3c(2-\nu)^2}{4}\frac{d^2v_n}{dx^2}\left[2z_0\left(\frac{dz_0}{dx}\right)^2 + (z_0^2-1)\frac{d^2z_0}{dx^2}\right]\right\} + N\frac{d^2v_n}{dx^2} + \frac{Eh}{R}\left[\frac{v_n}{R} - \frac{ch(2-\nu)}{8}(1+z_0)^2\frac{d^2v_n}{dx^2}\right] = 0 \quad (32)$$

$$\frac{d^2v_n}{dx^2} + \frac{f_2(z_0, c)}{Rh}v_n = 0 \quad (33)$$

where

$$f_2(z_0, c) = -\frac{2(1-\nu^2)}{(2-\nu)[z_0 - (c/4)(2-\nu)^2(1+z_0)^2]} \quad (34)$$

Denote quantities in regions where $\dot{\kappa}_x > 0$ with the subscript 1 and quantities in regions where $\dot{\kappa}_x < 0$ with the subscript 2. With particular values of N, it is possible to satisfy (28) and (29) simultaneously and (32) and (33) simultaneously with

$$\begin{aligned} z_0 &= \text{const} \\ v_n &= \alpha\sin(f/Rh)^{1/2}x + \beta\cos(f/Rh)^{1/2}x \end{aligned} \quad (35)$$

Choosing a coordinate system at the center of each incipient wave and using the symmetry condition $v_n(x) = v_n(-x)$ gives

$$\begin{aligned} v_{n1} &= \beta_1\cos(f_1/Rh)^{1/2}x_1 \\ v_{n2} &= \beta_2\cos(f_2/Rh)^{1/2}x_2 \end{aligned} \quad (36)$$

Before continuing with the preceding analysis where junction conditions must be satisfied, as well as insuring equality of N in (28) and (32), the question arises as to whether or not the separate occurrence of solutions (35) has any meaning. Observing that $\dot{M}_x = 0$ at the ends of a wave, in the spirit of the hinge model analysis, place hinge circles at either $x_1 = l_1$ or $x_2 = l_2$ where $v_n = 0$. The cylinder will then buckle purely outward or purely inward into a series of half sine waves of wavelength $2l_1$ or $2l_2$. If for a value of $\lambda < \lambda_{cr}$, Eq. (18), $2l_1$ compares favorably with (L/m) from (15), then one would be able to draw conclusions regarding the effect of unloading on the hinge model discussed earlier.

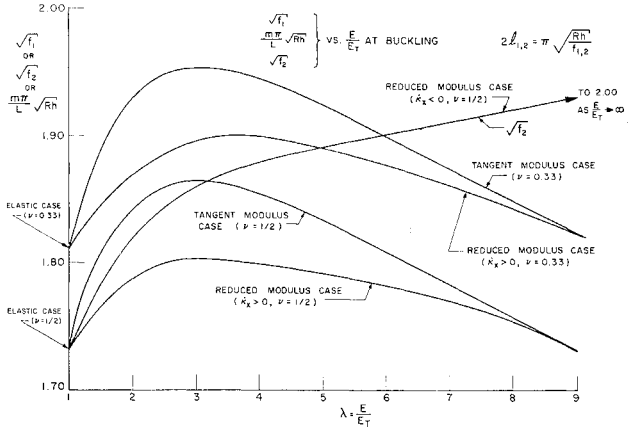

Fig. 5 Half-wavelengths for reduced modulus ($2l_1$ and $2l_2$) and tangent modulus (L/m) cases.

Calculations for the outward and inward wave hinge models are summarized in Figs. 4–6. Figure 4 gives the location of the elastic-plastic boundaries as a function of $\lambda = (E/E_T)$ at buckling. These curves were obtained by numerically solving fifth-order algebraic equations for z_{01} and z_{02}, which were arrived at by substituting (36) into (28) and (32) and then minimizing N with respect to z_{01} and z_{02}.

Figure 5 essentially compares the half-wavelength L/m obtained from Eq. (15) with $2l_1$ or $2l_2$ obtained from reduced modulus theory. For a given value of (E/E_T), the maximum difference between $2l_1$ and L/m is about $3\frac{1}{2}\%$. In point of fact however, the actual difference between $2l_1$ and L/m would be even smaller since tangent modulus theory and reduced modulus theory would not predict buckling at the same values of E/E_T.

Figure 6 is a plot of the nondimensionalized buckling stress $\sigma_{RM}/E(h/R)$ as a function of $\lambda = E/E_T$. For the outward wave and values of $\lambda \geq \lambda_{cr}$ Eq. (16) governs. Note the large difference between the buckling stresses for the inward and outward type hinge models at the same value of E/E_T. Although this comparison is not quite fair, this difference in stresses will prove important in what follows shortly.

In Fig. 7, the tangent modulus stress Eq. (16) is compared to the value obtained from reduced modulus theory, Fig. 6. For comparison, σ_{tan}/σ_{RM} for a column of rectangular cross section is also shown in the region $\lambda_{cr} \geqq \lambda \geqq 1$. Even for the same value of E/E_T there is only an extremely small difference (less than 2%) between σ_{tan} and σ_{RM} for the outward wave hinge model. Finally, we remark that, since $2l_1$ compares very favorably with L/m, it is evident that the effect of unloading makes only a negligibly small difference on the buckling load of the hinge model.

The separate solutions to the outward and inward wave hinge models can be combined to provide a solution for an actual perfect cylinder. It is evident from Fig. 6 that the minimum value of N as determined for the outward wave cannot occur. Since the minimum N for the inward wave is known corresponding to definite values of z_{02} and λ, a physically realizable z_{01} can be found insuring equality of N as computed from Eqs. (28) and (32). It then follows from (36) and the junctions insuring continuity of slope and displacement that

$$(f_1/Rh)^{1/2}l_1 = (f_2/Rh)^{1/2}l_2 = \pi/2$$
$$\frac{l_1}{l_2} = -\frac{\beta_1}{\beta_2} = -\frac{v_{n1}{}^{\min}}{v_{n2}{}^{\max}} = \left(\frac{f_2}{f_1}\right)^{1/2} \tag{37}$$

One result of matching solutions is shown in Fig. 8 where the very great tendency of the shell to buckle inward is noted. Since the variation of σ_{RM} with λ for this solution, Fig. 6 ($\kappa_x < 0$, $\nu = \frac{1}{2}$), can only have validity in the proportional limit region of the shell material, the pronounced inward

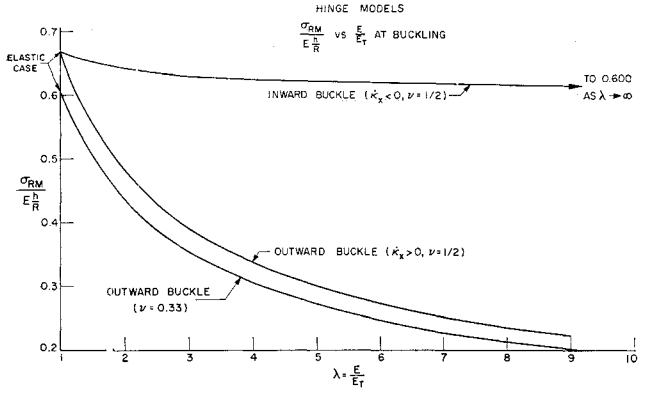

Fig. 6 Buckling stress for inward wave and outward wave hinge models.

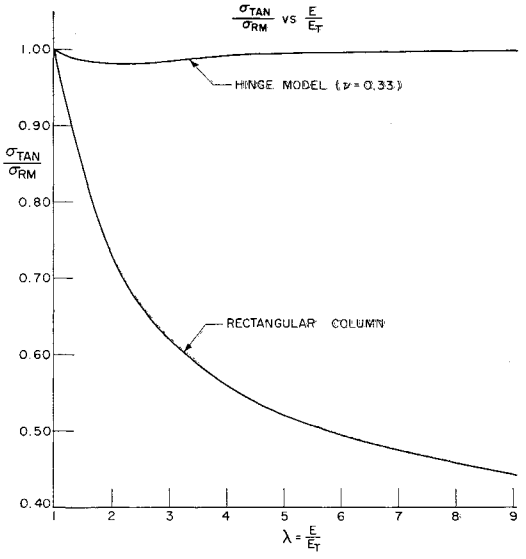

Fig. 7 Comparison of σ_{TAN}/σ_{RM} for outward wave hinge model and rectangular column.

type buckling observed in experiments in this region is thus not unexpected, even though it usually occurs in the characteristic diamond pattern.

Experiments on compressed cylindrical shells show that, above the proportional limit region, the shells buckle in an axisymmetric mode with the outward waves more pronounced than the inward waves. The analyses of the hinge models do suggest that the cylinder should show this pronounced outward buckling.

An approximate solution where continuity of slope is insured and which exhibits pronounced outward buckling can be obtained by assuming that in outward waves ($v_n < 0$) the material is loading everywhere, whereas for inward waves ($v_n > 0$), the material is unloading everywhere. These assumptions are indeed suggested by the hinge model trends but were, in fact, first proposed by Kuranishi.[3] The material in the inward wave cannot be unloading everywhere. Therefore this apparent artificial increase in the stiffness of the available deforming material will lead to a load that is not less than the true critical load. Choosing x_1 and x_2 oppositely directed, the junction conditions to be satisfied are

$$v_{n1}\big|_{x_1=l_1} = v_{n2}\big|_{x_2=l_2} = 0$$
$$\left.\frac{dv_{n1}}{dx_1}\right|_{x_1=l_1} + \left.\frac{dv_{n2}}{dx_2}\right|_{x_2=l_2} = 0 \tag{38}$$
$$\dot{M}_{x1}\big|_{x_1=l_1} = \dot{M}_{x2}\big|_{x_2=l_2}$$

Consistent with the assumptions, the differential equation governing the outward wave velocity v_{n1} is given by (13),

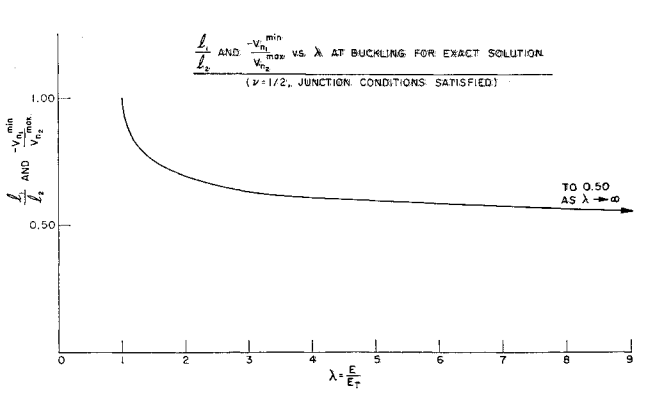

Fig. 8 Incipient wavelength and amplitude ratios for exact solution.

Table 1 Preliminary tests (1.306 in. $\leq R \leq$ 1.325 in.)

Cylinder	R/h	L/R	L, in.	h, in.	σ_{max}, psi	Remarks (see Fig. 14)
1	26.18	4.52	6.00	0.0506	58,600	Abrupt ends; loaded through ball and socket AX^a mode, outward wave more pronounced at top
2	26.44	6.78	9.00	0.0501	57,100	Same as #1
1A	26.18	2.60	3.45	0.0506	58,150	Cut from buckled cylinder #1; tested flat ended, AX mode
2A	26.44	1.51	2.00	0.0501	59,600	Cut from buckled cylinder #2; tested flat ended, AX mode
2B	26.44	2.95	3.91	0.0501	58,100	Same as #2A except loaded through ball and socket
3	26.56	0.75	1.00	0.0499	58,200	Tapered ends; loaded through ball and socket, AX mode
4	26.61	3.02	4.00	0.0498	58,200	Same as #3 except tested flat ended
5	25.94	0.76	1.00	0.0511	59,570	Uniform; tested flat ended; AX mode
6	25.88	0.38	0.50	0.0512	58,760	Same as #5
7	26.04	0.19	0.25	0.0509	...	No buckling failure; fracture at 79,250 psi (nominal)
8	114.56	1.53	2.00	0.0114	33,030	Uniform; load snapping elastic failure; inward DM^b pattern
9	116.61	0.77	1.00	0.0112	31,770	Same as #8
10	113.60	0.38	0.50	0.0115	35,600	Same as #8
11	121.25	0.19	0.25	0.0108	33,210	No discernible pattern at maximum load; further straining brings out beginnings of clear DM pattern

[a] AX = axisymmetric
[b] DM = diamond shaped.

whereas that governing the inward wave velocity v_{n2} is

$$K\frac{d^4v_{n2}}{dx_2^4} + N\frac{d^2v_{n2}}{dx_2^2} + \frac{Eh}{R^2}v_{n2} = 0 \tag{39}$$

where

$$K = \frac{Eh^3}{12(1-\nu^2)}$$

Since N can be bounded

$$N^2_{\tan} = \frac{4K_IEh}{R^2} < N^2 < \frac{4KEh}{R^2} = N^2_{\text{elastic}}$$

and $v_n(x) = v_n(-x)$ we have

$$\begin{aligned} v_{n1} &= \alpha_1 \cos fx_1 + \beta_1 \cos gx_1 \\ v_{n2} &= \alpha_2 \cosh(p+iq)x_2 + \beta_2 \cosh(p-iq)x_2 \end{aligned} \tag{40}$$

where α_1, α_2, β_1, and β_2 are constants, and

$$\begin{aligned} f &= \left\{\frac{N - [N^2 - (4K_IEh/R^2)]^{1/2}}{K_I(\lambda+3)/2}\right\}^{1/2} \\ g &= \left\{\frac{N + [N^2 - (4K_IEh)/R^2)]^{1/2}}{[K_I(\lambda+3)]/2}\right\}^{1/2} \\ p \pm iq &= \left\{\frac{-N \pm [N^2 - (4KEh/R^2)]^{1/2}}{2K}\right\}^{1/2} \end{aligned} \tag{41}$$

Satisfying the junction conditions (38) leads to four simultaneous equations for α_1, α_2, β_1, and β_2. Setting the determinant of these equations equal to zero results in

$$\frac{g\tan gl_1 - f\tan fl_1}{[K_I(\lambda+3)/4]\{g^2-f^2\}} + \frac{(p+iq)\tanh(p+iq)l_2 - (p-iq)\tanh(p-iq)l_2}{K\{(p+iq)^2-(p-iq)^2\}} = 0 \tag{42}$$

Two additional equations are obtained from (42) imposing the conditions that N be minimum with respect to l_1 and l_2. Hence,

$$\begin{aligned} g^2\sec^2 gl_1 - f^2\sec^2 fl_1 &= 0 \\ (p+iq)^2\operatorname{sech}^2(p+iq)l_2 - (p-iq)^2\operatorname{sech}^2(p-iq)l_2 &= 0 \end{aligned} \tag{43}$$

Equations (42) and (43) were solved numerically for N, l_1 and l_2. Once these values are known, it is not difficult to compute v_{n1} and v_{n2} to within a multiplicative constant. Results of calculations for Poisson's ratio equal to 0.33 are summarized in Figs. 9 and 10. The shell now shows a pronounced outward buckling (Fig. 9) for all values of (E/E_T).

The critical stress for the solution just obtained is compared to the tangent modulus stress, Eq. (16), in Fig. 10. For given values of (E/E_T) the ratio $(\sigma_{cr} - \sigma_{\tan})/\sigma_{\tan}$ is much smaller than the corresponding ratio $(\sigma_{RM} - \sigma_{\tan})/\sigma_{\tan}$ for say, a rectangular column. Since the actual spread between σ_{RM} and $\sigma_{\tan}$ for columns is usually too small to be of any real significance, Fig. 10 then indicates that the actual spread between σ_{cr} and $\sigma_{\tan}$ is insignificant for all except possibly very thick shells. In particular we note that this conclusion has been arrived at for a geometrically perfect shell.

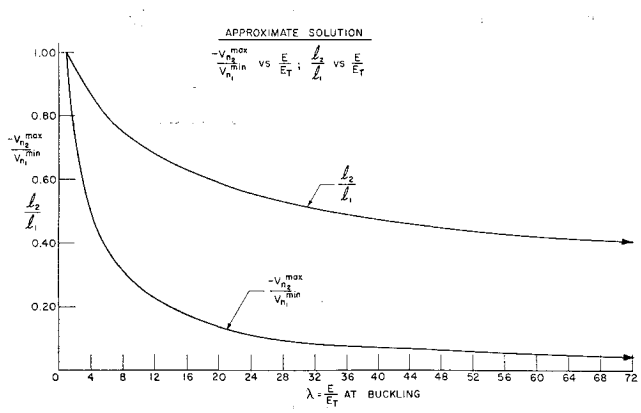

Fig. 9 Incipient wavelength and amplitude ratios for approximate solution.

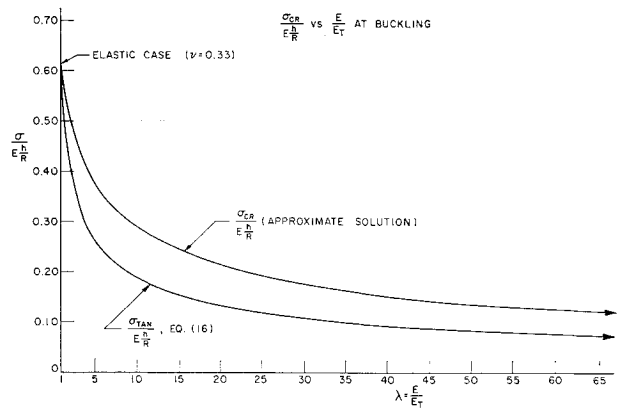

Fig. 10 Buckling stress for approximate solution compared to tangent modulus stress.

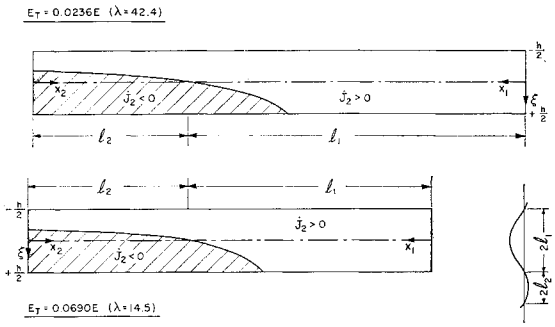

Fig. 11 Incipient regions of loading and unloading based on approximate solution.

Checking how closely the assumptions concerning the regions of loading and unloading are met leads to the scale drawings of Fig. 11 for two distinct values of λ. The assumption of loading is indeed an excellent assumption for the outward wave, whereas that of unloading is a good assumption for the inward wave. What is even more important, however, is that measurements made on the outer surface of the shell would indicate no evidence of stress reversal. This latter statement assumes that, at $\xi = -h/2$, the material in the outward wave, where $\dot{\kappa}_x > 0$, is loading. As for the hinge model, it is found that this conclusion is satisfied if buckling occurs at a value of $\lambda > 9$.

Another and perhaps the most important feature of the solution is that imposing kinematical constraints by forcing satisfaction of junction conditions does not significantly increase the buckling load over that found for the hinge model.

III. Experimental Investigation

A. Material Properties and Test Series

The base material from which all specimens were machined was 2024-T4 extruded aluminum tubing (3-in. o.d., $\frac{1}{4}$-in. wall). This alloy was chosen for its desirable machining properties and because it workhardens appreciably over the entire strain range of interest.

Longitudinal tensile coupons and longitudinal bending specimens were cut from widely separated sections of the 12-ft-long stock tube. The tensile specimens were approximately 0.10 × 0.25 in. in cross section with a 1-in. gage length. Pure bending specimens were 0.20 × 0.25 in. in cross section and approximately 5 in. in over-all length. Three lengths of the tubing approximately 4 in. long were used as compression specimens.

Average longitudinal data in tension and compression are summarized in Fig. 12. The nominal average ultimate stress in tension was 85,600 psi. Apart from the surprising

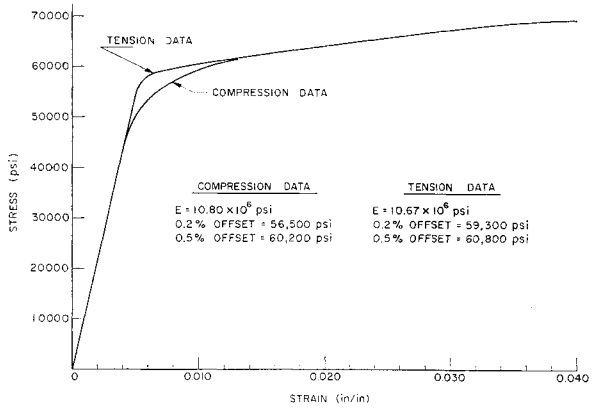

Fig. 12 Stress vs strain: average longitudinal data.

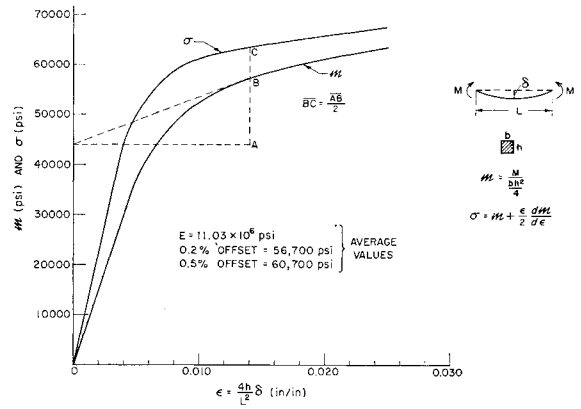

Fig. 13 Typical stress-strain curve obtained from pure bending test.

almost linear work-hardening behavior in tension depicted in Fig. 12, the 0.2% offset yield strength and the ultimate strength are far in excess of the respective guaranteed minimum values of 40,000 and 60,000 psi. The direct compression data is considered reliable for strains up to approximately 1.2%. This data shows considerably more rounding at the knee of the stress-strain curve than does the tension data.

A typical stress-strain curve obtained from a pure bending test is shown in Fig. 13. The rounding at the knee of the curve is due primarily to the behavior of the material in compression, but part is undoubtedly due to the graphical method of construction employed (illustrated in the figure). The curves obtained from the pure bending tests can be thought of as representing average behavior in tension or compression.

An extensive amount of preliminary testing was done in order to arrive at the best type specimen to use in the final tests. Figure 14 shows schematically the end conditions which were tried in the preliminary tests. Results of these tests are summarized in Table 1. Note in particular that the length of the specimen apparently has little effect on the buckling load. The exception to this statement is the very short specimen #7, which did not buckle. However, shell buckling was not expected for this specimen since the 0.25-in. length was smaller than the half wavelength predicted by (15) (approximately 0.45 in. in this case).

Based on the results of the preliminary tests, all specimens in the final test series were of the uniform type and were tested flat ended between smooth bearing blocks. Specimens were machined so that the ends were parallel to within ±0.0005 in. As a further excursion into the effect of end conditions on the buckling load, for some tests the bearing blocks were sprayed with either a molybdenum disulfide or fluorocarbon dry lubricant, whereas for other tests Teflon

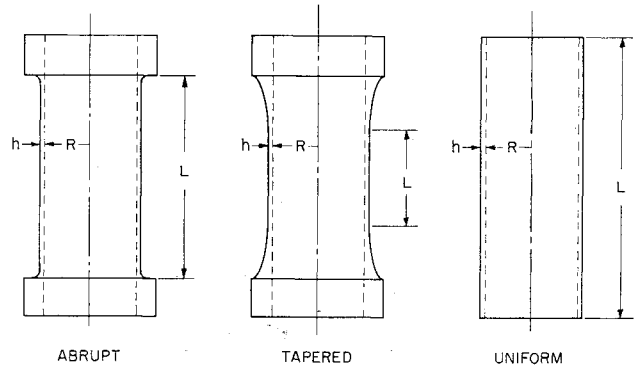

Fig. 14 End conditions.

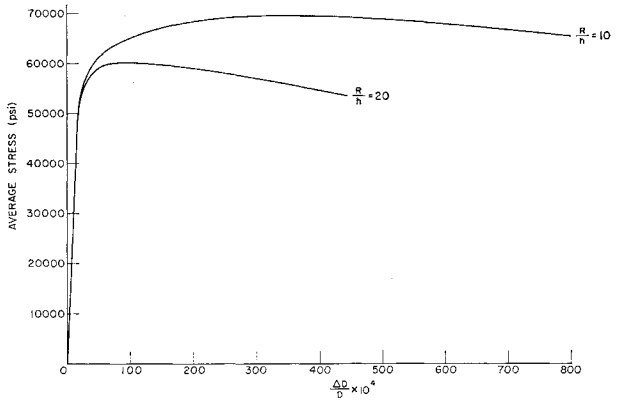

Fig. 15 Average stress vs change in diameter at center.

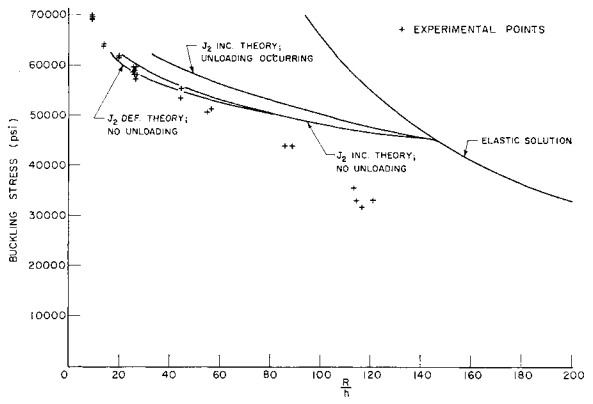

Fig. 16 Comparison of experiment and prediction based on longitudinal compression data.

sheets were inserted between the specimen and the bearing blocks. No consistent difference was noted.

Specimens were tested at slow strain rates in a 120,000-lb capacity Riehle testing machine. During a test, the over-all change in length was recorded as well as the change in diameter at the center of the specimen. Relevant geometrical parameters, maximum stresses, and mode of buckling, are summarized in Table 2. Typical curves of the average testing machine head movement vs the average direct stress are given in Fig. 2, whereas representative curves of average stress vs change in diameter for some of the thicker specimens are shown in Fig. 15. For the thicker specimens $(R/h) = 10$ and $(R/h) = 15$, time-dependent effects manifest themselves when the average stress entered well into the plastic range. The load was recorded after δ_{av}/L settled down to 0.0001/min or less. For these specimens the actual maximum stress reached during the loading process was approximately 2500 and 1500 psi, respectively, higher than listed in Table 2.

B. Comparison with Theory

The buckling stresses of Tables 1 and 2 are transferred to Fig. 16 for comparison with the theoretical curves based on longitudinal compression data. Theoretical predictions based on tension and compression data are compared in Fig. 17. The theoretical curves themselves exhibit two significant features. First, as expected, the difference between predictions of incremental theory accounting for unloading from the no unloading case is small in general. Second, predictions of incremental theory and deformation theory based on no unloading occurring in a perfect shell are very close over the entire range of (R/h) values. This is due in part to the dominance of the tangent modulus in predicting the buckling stresses. A small increase in stress gives a large decrease in tangent modulus. The choice of the axisymmetric buckling mode also enters into the closeness of the predictions. It is evident from the studies made by Gerard[22] and Lee[7] that for the diamond-shaped circumferential wave mode of buckling there will be large differences between the predictions of incremental and deformation theory. However, deformation theory is not as sensitive as incremental theory to the mode of buckling.

Experimental agreement with theoretical predictions is considered to be excellent for $(R/h) < 40$ and good for $(R/h) < 60$. Although this in itself is a small range, it is the range where classical stability was expected to be useful. In a crude sense, the no-unloading incremental theory curve is a reasonable prediction of the buckling stress following the concept of Shanley. For $60 > (R/h) > 40$ initial imperfections would provide better agreement with theory. For $(R/h) > 80$ there is a marked difference between experiment and the theory as presented. Buckling occurred catastrophically in a diamond shaped mode reminiscent of elastic buckling.

All shells that buckled in an axisymmetric pattern showed a definite tendency toward pronounced outward buckling. Specimen #21 did not buckle, which was expected since the 0.50-in. length was much smaller than $(L/m) \approx 1.0$ in. as computed from (15).

The experimental points exhibit comparatively little scatter in the range $(R/h) < 60$ where plastic buckling occurred. This is attributed partly to the care used in the preparation

Table 2 Final test series (1.358 in. $\leq R \leq$ 1.400 in.)

Cylinder	R/h	L/R	L, in.	h, in.	σ_{max}, psi	Remarks
12	9.70	2.92	4.00	0.1412	69,630	AX[a] mode
13	14.02	1.43	2.00	0.0999	64,110	AX mode
14	19.71	0.72	1.00	0.0703	61,580	AX mode
15	44.69	1.47	2.00	0.0306	55,490	Transition mode; AX near ends, gentle DM[b] pattern in central region
16	56.52	0.73	1.00	0.0241	51,380	Well-defined inward DM pattern
17	89.33	1.47	2.00	0.0152	43,950	Snapping failure; inward DM pattern
18	9.76	2.92	4.00	0.1404	70,000	AX mode
19	9.76	1.09	1.50	0.1403	69,320	AX mode
20	9.76	0.73	1.00	0.1404	69,840	AX mode
21	9.76	0.37	0.50	0.1404	...	Loaded to 96,000 psi (nominal); noticeable barreling but load did not reach a maximum
22	13.93	0.72	1.00	0.1005	63,790	AX mode
23	19.66	1.44	2.00	0.0705	61,480	AX mode
24	44.19	0.73	1.00	0.0309	53,380	AX mode with some irregularities
25	54.93	1.47	2.00	0.0248	50,640	Transition mode similar to #15
26	85.95	0.74	1.00	0.0158	43,690	Same as #17
27	9.70	2.92	4.00	0.1413	69,230	AX mode

[a] AX = axisymmetric.
[b] DM = diamond shaped.

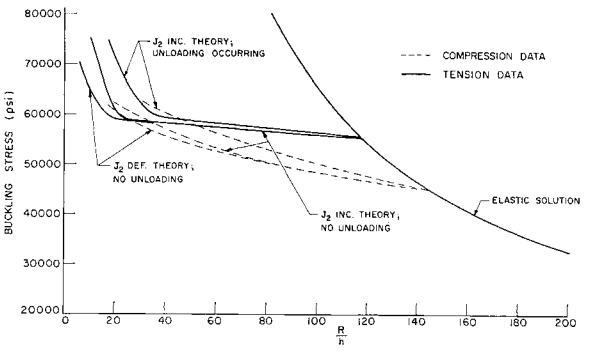

Fig. 17 Comparison of theoretical predictions.

and testing of the specimens but is strong evidence that small geometric imperfections in shape, which always exist, do not have a large effect on the buckling strength. However, the effect is measurable and probably does account for the points falling below the incremental theory curve.

IV. Conclusions

An analysis coupled with an experimental program shows that classical (perfect geometry) stability concepts are useful in predicting plastic buckling loads and the geometry of buckling for axial compression of fairly thick cylindrical shells, radius to thickness ratios less than 60. To extend the range, it is necessary to include initial imperfections in the analysis and employ Shanley's concept of considering the growth of disturbances all along the loading path until a maximum load is reached. The experiments also show that buckling strength is independent of length if the shell is longer than the half wavelength predicted by incremental theory.

Predictions of J_2 deformation theory and J_2 incremental theory are very close with deformation theory always predicting a slightly lower stress, for the perfect cylinder, than incremental theory. This result complements that found by Onat and Drucker[15] at the opposite extreme of plastic buckling behavior. In their study of the cruciform and related shapes, small initial imperfections or disturbances play the key role both in the proper approach using an incremental theory and in the explanation for the usual success of deformation theory based on perfect geometry. Although the reasoning, therefore, is very different in detail, the conclusion is the same and understandable in physical and mathematical terms. Good approximations to buckling loads are obtained when an actual elastic-plastic structural metal (incremental theory) is replaced by a nonlinear elastic material (deformation theory). Of course, as implied by Fig. 16, for $R/h > 80$, when imperfections would have a large influence on purely elastic buckling, they must be considered in a deformation theory as well.

An important result of the analysis is that imposing kinematic constraints by forcing satisfaction of junction conditions and accounting for unloading does not lead to a significant increase in the buckling load calculated for the hinge model. Furthermore, for the hinge model itself when $1 < \lambda < \lambda_{cr}$, the effect of unloading raises the buckling load by only a negligibly small amount.

References

[1] Shanley, F. R., "Inelastic column theory," J. Aeronaut. Sci. **14**, 261–268 (1947).

[2] Timoshenko, S. P. and Gere, J. M., *Theory of Elastic Stability* (McGraw Hill Book Co., Inc., 1961).

[3] Bijlaard, P. P., "A theory of plastic stability and its application to thin plates of structural steel," Proc. Koninkl. Ned. Akad. Wetenschap. **41**, 731–743 (1938).

[4] Bijlaard, P. P., "On the plastic stability of thin plates and shells," Proc. Koninkl. Ned. Akad. Wetenschap., **50**, 765–775 (1947).

[5] Bijlaard, P. P., "Theory and tests on the plastic stability of plates and shells," J. Aeronaut. Sci. **16**, 405–408 (1949).

[6] Gerard, G., "Compressive and torsional buckling of thin-wall cylinders in yield region," NACA TN3726 (August 1956).

[7] Lee, L. H. N., "Inelastic buckling of initially imperfect cylindrical shells subject to axial compression," J. Aerospace Sci. **29**, 87–95 (1962).

[8] Kuranishi, M., "The buckling stress of thin cylindrical shell under axial compressive load, forming axial-symmetrical deformation," J. Soc. Appl. Mech. Japan **3**, 139–144 (1950).

[9] Drucker, D. C., "Plasticity," *Structural Mechanics* edited by J. N. Goodier and N. J. Hoff (Pergamon Press, New York, 1960).

[10] Budiansky, B., "A reassessment of deformation theories of plasticity," J. Appl. Mech. **26**, 259–264 (June 1959).

[11] Drucker, D. C., "A more fundamental approach to plastic stress-strain relations," *Proceedings 1st National Congress for Applied Mechanics* (American Society of Mechanical Engineers, New York, 1951), pp. 487–491.

[12] Handelman, G. H. and Prager, W., "Plastic buckling of a rectangular plate under edge thrusts," NACA Rept. 946 (1949).

[13] Prager, W., "Theory of plastic flow vs. theory of plastic deformation," J. Appl. Phys. **19**, 540–543 (1948).

[14] Drucker, D. C., "Stress-strain relations in the plastic range—A survey of theory and experiment," Brown University, Div. of Applied Mathematics, Office of Naval Research Contract N7onr-358 (December 1950).

[15] Onat, E. T. and Drucker, D. C., "Inelastic instability and incremental theories of plasticity," J. Aeronaut. Sci. **20**, 181–186 (1953).

[16] Drucker, D. C. and Onat, E. T., "On the concept of stability of inelastic systems," J. Aeronaut. Sci. **21**, 543–549 (1954).

[17] Gerard, G. "On the role of initial imperfections in plastic buckling of cylinders under axial compression," J. Aerospace Sci. **29**, 744–745 (1962).

[18] Gerard, G. "Compressive stability of orthotropic cylinders," J. Aerospace Sci. **29**, 1171–1179 (1962).

[19] Batterman, S. C., "Load-deformation behavior of shells of revolution," Proc. Am. Soc. Civil Engrs., J. Eng. Mech. Div. **90**, 1–19 (December 1964).

[20] Flugge, W., *Stresses in Shells* (Springer-Verlag, Berlin, 1960).

[21] von Kármán, T., *Forschungsarbeiten* (Berlin, 1910); also Ref. 2.

[22] Gerard, G., "Plastic stability of geometrically orthotropic plates and cylindrical shells," New York Univ. TR SM61-11 (July 1961).